DIRECT NUMERICAL SIMULATION OF INTERACTIONS BETWEEN A MIXING LAYER AND A WAKE AROUND A CYLINDER

Eric Lamballais *
Laboratoire d'Etudes Aérodynamiques UMR 6609, Université de Poitiers/CNRS
Téléport 2 - Bd. Marie et Pierre Curie B.P. 30179
86962 Futuroscope Chasseneuil Cedex, France, lamballais@univ-poitiers.fr

Jorge Hugo Silvestrini
Departamento de Engenharia Mecânica e Mecatrônica, Faculdade de Engenharia
Pontifícia Universidade Católica do Rio Grande do Sul
Av. Ipiranga 6681, 90619-900 Porto Alegre - RS, Brasil, jorgehs@em.pucrs.br

ABSTRACT

Direct Numerical Simulation of turbulent flows around a cylinder are performed using the virtual boundary technique to modelize the presence of the obstacle. Such a method consists in the imposition of a no-slip boundary condition within the flow field by the use of a specific forcing term added to the momentum equation. In this paper, we consider the flow around a single cylinder with upstream conditions corresponding to a constant velocity flow or to a mixing layer flow. In the first case, the usual one, common features of the cylinder wake dynamics are recovered (three-dimensional vortex shedding) showing the ability of the virtual boundary technique (coupled to an accurate finite difference method) to take obstacles into account realistically despite the use of a simple Cartesian grid. The second case can be basically decomposed in three main flows : a low-speed wake, a high-speed wake and a mixing layer flow. It is found that interaction mechanisms between these three flows are predominant. The cylinder induces a strong distortion on the spatial development of the mixing layer. Analysis of the mean flow shows the presence of strong upward and downward streams respectively in front of and behind the cylinder. In the regions of slow/fast wakes, vortex shedding are found at frequencies which seem to be linked. Vortex dynamics analysis shows that large scale eddies are the key element of the interaction mechanisms.

*Simulations were carried out at the IDRIS, the computational center of the CNRS. This study was partially supported by the Cemagref (Rennes). We are grateful to D. Heitz and E.B. Camano Schettini for helpful comments on this work, J. Delville, G. Arroyo and J.P. Bonnet for informative discussions.

INTRODUCTION

Computation of turbulent complex flows is a challenge for Direct Numerical Simulation (DNS) or Large Eddy Simulation (LES). Schematically, the main difficulty is to obtain an accurate description of the turbulent structure dynamics in presence of complex body geometries. In engineering flow simulations, the description of the external geometry is traditionally favoured by the use of body-fitted curvilinear or unstructured grids. The major drawbacks of such approach are a considerable increase of the computational cost and a significant deterioration of the accuracy. On the opposite side, when regular grids are used, an efficient code can be used (in terms of computational cost and accuracy) but is *a priori* limited to simplified geometries. This paper presents results obtained from an alternative approach which consist in the use of an accurate numerical code to perform simulations of complex geometry flow on a regular grid. Such a possibility is offered by the immersed-boundary technique (see Fadlun *et al.*, 2000 for recent developments) which is treated here by the introduction of a body-force field in the momentum equation.

FLOW CONFIGURATION AND NUMERICAL METHODS

Flows around a circular cylinder of diameter D are considered in a Cartesian frame of reference $\mathcal{R} = (0; x, y, z)$. The cylinder axis is oriented along the vertical direction y at the intersection between the streamwise section x_{cyl} and the spanwise one $z = 0$ (see figure 1). At the inflow section, a plane mixing

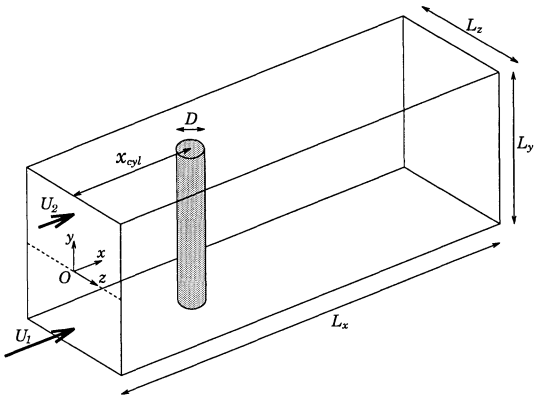

Figure 1: Schematic view of the flow configuration

layer flow between two streams of velocities U_1 and U_2 is imposed, the associated mean shear being aligned with the y-direction. We note u_x, u_y, uz the velocity components and ν the kinematic viscosity. A mean velocity profile $\langle u_x \rangle (y)$ is imposed at $x = 0$ using an hyperbolic tangent with

$$\langle u_x \rangle (y) = \frac{U_1 + U_2}{2} - \frac{U_1 - U_2}{2} \tanh\left(\frac{2y}{\delta_{\omega_i}}\right)$$

where δ_{ω_i} is the inflow vorticity thickness. The difference and convective velocities are respectively noted $\Delta U = U_1 - U_2$ and $U_c = (U_1 + U_2)/2$. The three fundamental non-dimensional parameters of the present problem are the ratio of velocities $\lambda = \Delta U/2U_c$, the Reynolds number $Re = U_c D/\nu$ and the ratio of lengths $H = D/\delta_{\omega_i}$. At the downstream of the cylinder, the present flow leads to an interaction between a mixing layer and a wake of orthogonal mean shear directions (three-dimensional mean flow without any homogeneous direction). In addition, the wake can be itself divided schematically in a high-speed wake for $y < -\delta_\omega/2$ and a low-speed wake for $y > \delta_\omega/2$. Note that small values for λ correspond to flow regimes where mixing layer effects are moderate, while the case $\lambda = 0$ denotes the case where a simple uniform flow is imposed at the inflow section. In this paper, two cases are considered with $\lambda = 0$ or $\lambda = 0.5$ (with $H = 3$), all other configuration parameters being the same with $Re = 300$, $x_{cyl} = 13D$ and $(L_x, L_y, L_z) = (28D, 16D, 8D)$.

The incompressible Navier-Stokes equations are directly solved using a computational grid of $505 \times 193 \times 144$ points in non-staggered configuration. Sixth-order compact centered difference schemes are used (Lele, 1992) to evaluate all spatial derivatives, except near the in- and outflow boundaries where single sided schemes are employed for x-derivative calculation. Note that these numerical schemes have very limited anisotropic errors (Lele, 1992), this quality being crucial for present calculations where the computational grid do not fit the mean directions of the flow. Free-slip boundary conditions are applied at $y = \pm L_y/2$ using symmetry and anti-symmetry considerations while periodicity is imposed in the z-direction. The outflow boundary condition ($x = L_x$) is deduced by solving a simplified convection equation on the exit plane. For inlet conditions, small random perturbations with a given kinetic energy spectrum are superimposed on the inflow mean velocity profile to mimic the residual turbulence. For the two simulations presented here, the kinetic energy spectrum peaks at the fundamental mode of the mixing layer predicted by linear stability theory. Time integration is performed with a third-order low-storage Runge-Kutta method.

The imposition of no-slip boundary condition due to the cylinder is performed using the virtual boundary technique originally proposed by Goldstein *et al.* (1993). This approach allows the imposition of no-slip boundary condition within the flow field by a feed-back unsteady forcing term added to the momentum equation. These forces are chosen to lie along a desired surface and to have a magnitude and direction opposed to the local flow. For present numerical methods, the use of accurate centered schemes for spatial discretization (without numerical dissipation) impose a particular care in the treatment of the forcing. Hence, if the forcing term is not smooth enough in space, significant spatial oscillations are produced. To reduce this problem, we follow the procedure proposed by Goldstein *et al.* (1993) (in the context of spectral methods) by the use of a spatial smoothing and filtering. The smoothing is applied to the force field in order to reduce the discontinuity associated to the boundary. As Goldstein *et al.* (1993), a Gaussian distribution is used to reduce by more than 63 % the force of the grid points adjacent and outside to the cylinder, while the force of other external points is essentially zero. The spatial filtering is applied to the non-linear and forcing terms using the same compact filter in the three directions of space. Filter coefficients are chosen to preserve the global accuracy of spatial discretization (sixth order) and to affect only the smallest scales of the flow (Lele, 1992). Note that the use of this filtering procedure avoid the accumulation effect which occurs when successive filtering are applied directly to the solution.

Validations

The validation of present numerical methodology has been performed considering various Reynolds numbers cases with $\lambda = 0$ and different computational domain sizes. All these preliminary calculations were purely two-dimensional and used an isotropic grid with $\Delta x = \Delta z$. At very low Reynolds number, the critical value $Re \approx 50$ corresponding to the onset of wake instability leading to vortex shedding is satisfactory recovered. For $Re = 200$ and $Re = 300$, when mesh sizes are respectively $D/12$ and $D/18$, we find that the Strouhal number $St = fD/U_c$ (f: frequency of the vortex shedding) is under-estimated by around 20 % compared to the well accepted values in the literature (Williamson, 1996). We observe that a grid refinement avoid this problem. The mean velocity field examination shows clearly that in practice, the combined effects of the forcing and the filtering tend to freeze the fluid on an effective cylinder diameter D_e larger that the expected one, with $D_e \approx 1.2D$ for a mesh size of $D/18$. Such an increase can be related to the uncertainty on the exact position of the cylinder boundary associated partially to the smoothing of the forcing term (this point has already been noted by Goldstein *et al.*, 1993). Then, main statistical data (St, turbulent intensities) are found to be more consistent if D_e is used as length scale. A good solution (not exploited for present results) would be to anticipate, at a given resolution, the value of D_e when the Reynolds number and domain size are prescribed. Here, for clarity, all results are normalized with D but can naturally be easily rescaled using the ratio D_e/D=1.2 for comparison with previous experimental or numerical works. A last remark concerns the confinement effect due to the periodic boundary conditions in z-direction. In two-dimensional simulations, we found that $L_z = 8D$ was large enough to not perturb the streamwise development of the wake vortices. However, for the three-dimensional case, the vortex organization lead to an increase of the wake expansion so that for $L_z = 8D$, a moderate confinement effect is expected as we will see in the following section.

WAKE DUE TO AN UNIFORM FLOW

Figure 2 shows perspective view of the vorticity modulus denoting the vortical organization of the flow. The instant of this picture corresponds to the end of the simulation $t = 92D/U_c$, the time necessary to a structure convected with the velocity U_c for covering 6 times the distance $L_x - x_{cyl}$. Here, all the key structures of a turbulent wakes seem to be reproduced. A three-dimensional vortex shedding is clearly observed with a simultaneous stretching of streamwise vortex pairs (mode-B; see Williams, 1996). Note that free-slip boundary conditions at $y = \pm L_y/2$ do not forbid the occurrence of oblique vortex shedding which are found to be weakly non-parallel at various times during the simulation. The spanwise wavelength λ_y of the streamwise vortex pair formation is in good agreement with previous experimental or numerical studies (Williamson, 1996) with $\lambda_y \approx 1.3D$.

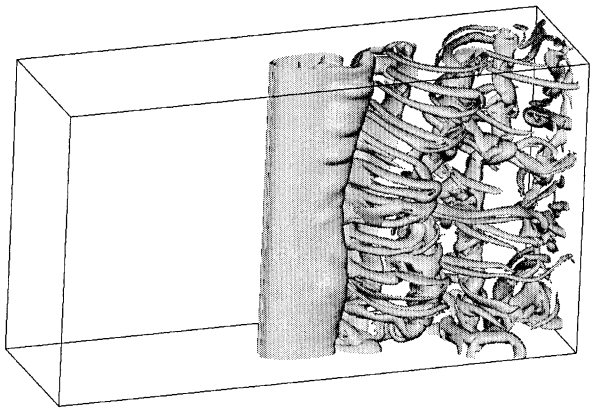

Figure 2: Perspective view of an isosurface $\omega = 1.5U_c/D$ of vorticity modulus ($\lambda = 0$).

A temporal sequence of $44D/U_c$ corresponding to 8 shedding cycles has been used to estimate the Strouhal number ($St = 0.18$) and the turbulent statistics. Main statistical data are summarized in table 1 with a comparison with experimental data of Noca *et al.* (1998) at two different Reynolds numbers. The ability of present numerical methodology using immersed-boundary technique to obtain consistent statistical data is here confirmed, especially if data are rescaled using D_e. Note that the present over-estimation of the length formations $L_{R_{ij}}$ (defined as the streamwise location where the Reynolds stress $R_{ij} = \left\langle u_i' u_j' \right\rangle$ reaches a maximum) has already been observed in DNS of Mittal and Balachandar (1995) where a body fitted grid was used. Here, we interpret these tendencies as the consequence of the confinement effect due to the limited computational size in z-direction.

WAKE DUE TO A MIXING LAYER FLOW

Such a complex flow, used for ultra-clean protection in the food industry, was studied

	Present DNS	Noca *et al.* DPIV	Noca *et al.* DPIV
Re	300	390	1260
$L_{R_{xx}}/D$	2.6	1.45	2.01
$L_{R_{zz}}/D$	3.4	2.01	2.61
$L_{R_{xz}}/D$	3.2	1.84	2.47
$\max[R_{xx}]/U_c^2$	0.16	–	0.12
$\max[R_{zz}]/U_c^2$	0.34	–	0.32
$\max[R_{xz}]/U_c^2$	0.10	–	0.09

Table 1: Comparison of present maximum Reynolds stresses (streamwise positions and values) with experimental data of Noca *et al.* (1998) obtained by Digital Particle Image Velocimetry (DPIV).

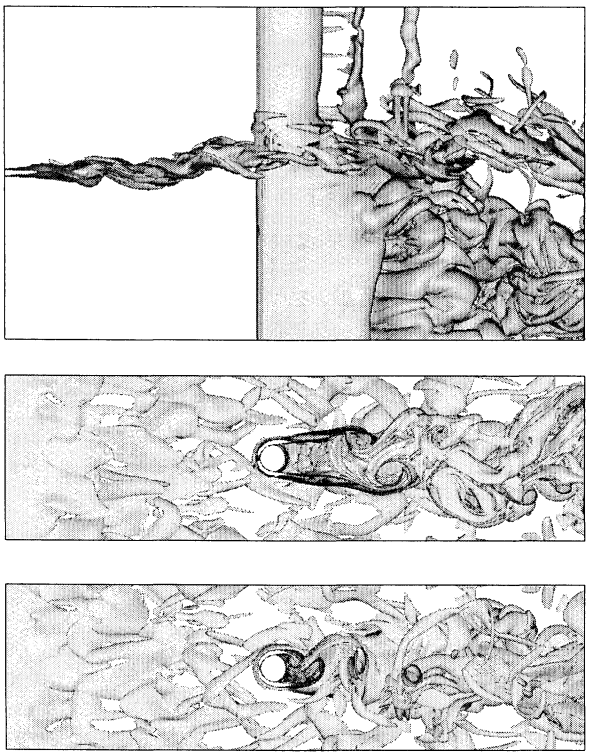

Figure 3: Side, bottom and top views showing an isosurface $\omega = 1.5U_c/D$ of vorticity modulus ($\lambda = 0.5$).

experimentally by Heitz (1999) (see also Heitz *et al.*, 1997). Despite the higher Reynolds numbers ($Re = 3330, 7500$) considered in this study, a comparison with present results will be given here. Figure 3 shows side, bottom and top views of the vorticity modulus at the final time of the simulation $t = 114D/U_c$. These views show, from left to right, the roll-up and pairing of Kelvin-Helmholtz structures of the mixing layer in front of the cylinder and the development of a complex wake behind it.

On the side view, a significant curvature of the mixing layer can be observed just in front of the cylinder. This upward shift of the the mixing layer is consistent with experimental observations of Heitz (1999), who associated this deviation to a negative vertical pressure gradient just in front of the cylinder. The inverse tendency is also recovered immediately behind the cylinder where the fluid follows a strong downward motion. These tendencies can be observed on figure 4 where positive and negative isosurfaces of mean vertical velocity $\langle u_y \rangle$ are presented. Note that the bracket operator indicates here an average in time using the final temporal sequence $44D/U_c$ and the Oxy-plane symmetry.

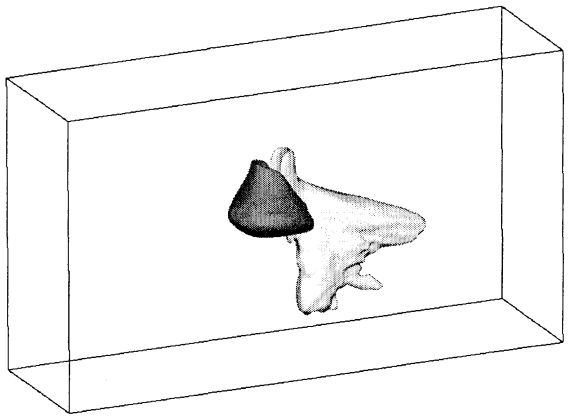

Figure 4: Perspective view of isosurfaces $\langle u_y \rangle = \pm 0.25U_c$ of mean vertical velocity. Dark surface corresponds to positive value ($\lambda = 0.5$).

The analysis of the vortical structure of the flow at successive instants shows clearly that vortex shedding occurs in the high-speed and low-speed regions of the wake. The Karman vortex dynamics of the slow wake in the region $L_y/4 < y < L_y/2$ corresponds qualitatively to a low Reynolds wake with a local Reynolds number $U_2 D/\nu = 150$ and a local Strouhal number $St_2 = f_2 D/U_2 \approx 0.18$. These values can be compared to the fast wake ones (for $-L_y/2 < y < -L_y/4$) with $U_1 D/\nu = 450$ and $St_1 = f_1 D/U_1 \approx 0.14$. Note that present Strouhal numbers are only approximate due to the very limited shedding cycle numbers considered to evaluate them (we count around 4 and 9 shedding cycles in the slow wake and fast wake respectively). The decrease of St_1 compared to the value $St \approx 0.2$ shows that the fast wake dynamics is linked to the mixing layer and/or the slow wake dynamics. The mean downward motion behind the cylinder is probably the stamp of these interaction mechanisms. This modification of the natural frequency of the fast wake suggests that vortex shedding in the high-speed region of the flow could be synchronized by mixing layer/slow wake instationarities. It is interesting to note that in first approximation, we have the relations $f_1 \approx 2f_2$ and $f_{ml} \approx 2f_1$ where f_{ml} is the main frequency of the mixing layer just upstream to the

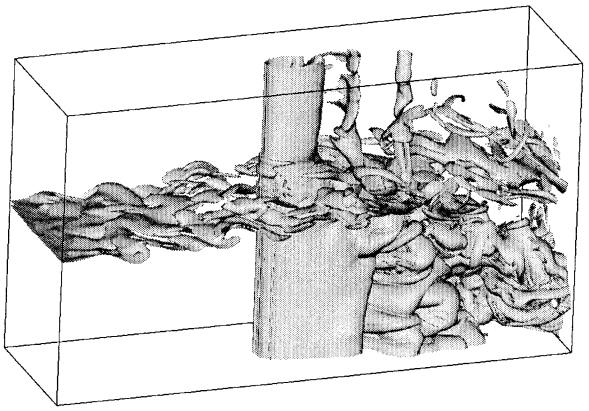

Figure 5: Perspective view of an isosurface $\omega = 1.5U_c/D$ of vorticity modulus ($\lambda = 0.5$).

cylinder. To confirm the link between these frequencies, this simulation have to be continued in order to increase the number of turbulent events and to obtain more reliable informations about temporal scales of the flow. It is also worth to observe that even if vortex shedding is present in the fast wake, vortical structures are clearly less organized than in the slow wake region or for the wake alone (see figure 2 for comparison with figure 5). Another remark concerns the streamwise location where eddies roll-up to form Karman vortices, which is considerably more downstream in the high-speed region of the wake. Moreover, animations of the flow shows that vortex shedding is irregular in time while alternate Karman vortices (of opposite rotation) do not form systematically out of phase.

Karman vortices are found to be oblique with respect to the y-direction, with an angle increasing during the downstream development of the flow. This behaviour seems to be due to the velocity differences $U_1 - U_c$ and $U_c - U_2$, Karman vortices being transported with a convection velocity varying from U_i $(i = 1, 2)$ to U_c when y goes to 0. According to this schematic view, it can be anticipated that the velocity ratio λ is the main parameter to determine the inclination angle of the Karman vortices. Note that Karman structures crossing the mixing layer seem to be present but are rather delicate to identify due to the small scale turbulence in the mixing layer. If their existence was confirmed, it would demonstrate the occurrence of synchronization mechanisms between the slow and fast wakes, may be through viscous reconnection in the core of mixing layer.

In order to compare quantitatively the main spatial scales in the slow and fast wakes, two xz-maps of the Reynolds stress R_{zz} at two y-

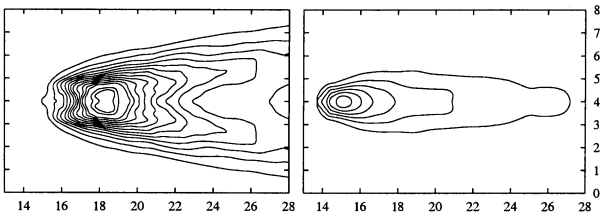

Figure 6: Isocontours (0.025 to 0.4 by step of 0.025) of $\langle u'_z u'_z \rangle / U_c^2$ at $y = -L_y/4$ (left) and $y = L_y/4$ (right).

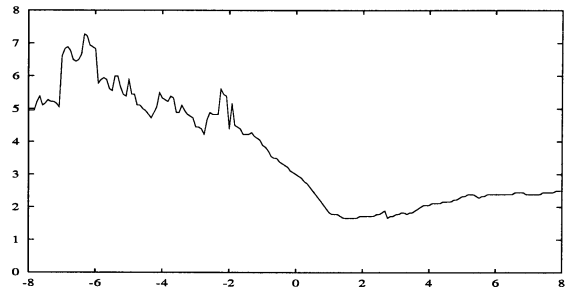

Figure 7: Profile of the length formation $L_{R_{zz}}$ along y

locations are presented in figure 6. Fluctuation levels are naturally higher in the fast wake and do not coincide with the slow wake ones even if data are rescaled using U_1 for $y = -L_y/4$ and U_2 for $y = L_y/4$. More precisely, using such a local scaling, we observe an important increase of $\left\langle u'_y u'_y \right\rangle$ in the fast wake and a decrease of the two other fluctuating velocity components (see table 2). This tendency confirms the more three-dimensional character of the fast wake dynamics which is strongly perturbed by the intense downward fluid motion behind the cylinder. The streamwise location of the maximum values of R_{zz} is found to strongly increase in the high-speed region of the wake. Here, due to the inhomogeneity in the y-direction, the formation length (based here only on u'_z for simplicity) is dependent of this coordinate. Such a profile $L_{R_{zz}}(y)$ is presented on figure 7. The irregular character of this profile (particularly for $y < 0$) can be attributed to a lack of convergence amplified by the elongated shape of R_{zz} iso-values in the x-direction which tends to increase the uncertainty about the precise position of the maximum value. Figure 7 shows however that the formation length is strongly modified by the mixing layer with schematically two regions

	$y = -L_y/4$ $(i = 1)$	$y = L_y/4$ $(i = 2)$
$\max[R_{xx}]/U_i^2$	0.12	0.17
$\max[R_{yy}]/U_i^2$	0.15	0.08
$\max[R_{zz}]/U_i^2$	0.27	0.34

Table 2: Comparison of maximum normal Reynolds stresses at $y = -L_y/4$ and $y = L_y/4$ using a local normalization by U_1 and U_2 respectively.

with $L_{R_{zz}} \approx 5$ in the high-speed region and $L_{R_{zz}} \approx 2.5$ in the low-speed region. These important increase of formation length in the fast wake is in good qualitative agreement with the experiments of Heitz (1999) despite the moderate value of the Reynolds number used here. The global qualitative agreement of present results with experiments suggests that the main features of this complex flow are not strongly dependent of the Reynolds number and can be examined accurately using DNS in order to better identify the vortical structures associated to the interaction mechanisms between the mixing layer and the wake.

CONCLUSION

In this work, it is shown that an accurate numerical code coupled to the immersed-boundary technique allows to perform DNS of turbulent flows in presence of a single cylinder with a geometry which is not *a priori* well designed for the simple Cartesian grid used here. It is interesting to note that the use of such a simplified grid is not only attractive in terms of accuracy and simplicity for DNS. It could also be helpful in the LES context where the formalism is better defined when accurate numerical methods are used on orthogonal and homogeneous grids (Ghosal, 1995, 1996). Moreover, such a computational configuration allows the use of efficient subgrid models derived from spectral space formulations (Lesieur, 1997, Lesieur and Métais 1996). Here, it is shown that a realistic turbulent flow dynamic can be obtained in the presence of a single cylinder. The interaction between a mixing layer and a wake (generated by the cylinder) is also considered. The mean structural features of this complex flow already observed experimentally are here satisfactory recovered numerically. This is the first time, in our knowledge, that such a three-dimensional complex flow is reproduced by DNS. Analysis of the vortex dynamics suggests that large scale eddies are decisive in the interaction mechanisms between the wakes and the mixing layer. It is however somewhat delicate to establish clearly these interactions due to the complex nature of such a flow and its considerable number of degrees of freedom. Further investigations on this subject require the use of a specific technique for coherent structure eduction. For this purpose, the use of Proper Orthogonal or Wavelet Decompositions (Delville *et al.*, 2000; Farge *et al.*, 1992) applied to instantaneous three-dimensional fields could be helpful to analyze the nature of the synchronization mechanisms.

REFERENCES

J. Delville, E. Lamballais, and J.P. Bonnet. POD, LODS and LSE: their links to control and simulations of mixing layers. *ERCOFTAC Bulletin*, 46, 2000.

E. A. Fadlun, R. Verzico, P. Orlandi, and J. Mohd-Yusof. Combined immersed-boundary finite-difference methods for three-dimensional complex flow simulations. *J. Comp. Phys.*, **161**:35–60, 2000.

M. Farge. Wavelet transforms and their applications to turbulence. *Ann. Rev. Fluid Mech.*, **24**:395–457, 1992.

S. Ghosal. An analysis of numerical errors in large-eddy simulations of turbulence. *J. Comp. Phys.*, **125**:187–206, 1996.

S. Ghosal and P. Moin. The basic equations for the large eddy simulation of turbulent flows in complex geometry. *J. Comp. Phys.*, **118**:24–37, 1995.

D. Goldstein, R. Handler, and L. Sirovich. Modeling a no-slip boundary condition with an external force field. *J. Comp. Phys.*, **105**:354–366, 1993.

D. Heitz. *Etude expérimentale du sillage d'un barreau cylindrique se développant dans une couche de mélange plane turbulente.* PhD thesis, Université de Poitiers, 1999.

D. Heitz, J. Delville, G. Arroyo, J.H. Garem, J.P. Bonnet, and P. Marchal. Interaction of the wake of a circular cylinder and a plane mixing layer. In *Proc. 11th Symp. on Turbulent Shear Flows*, pages 5–1–5–6, 1997.

S. K. Lele. Compact finite difference schemes with spectral-like resolution. *J. Comp. Phys.*, **103**:16–42, 1992.

M. Lesieur. *Turbulence in fluids.* Kluwer Academic Publishers, third edition, 1997.

M. Lesieur and O. Métais. New trends in large-eddy simulations of turbulence. *Ann. Rev. Fluid Mech.*, **28**, 1996.

R. Mittal and S. Balachandar. Effect of three-dimensionality on the lift and drag of nomally two-dimensional cylinders. *Phys. Fluids*, **7**:1841–1865, 1995.

F. Noca, H.G. Park, and M. Gharib. Vortex formation length of a circular cylinder ($300 < Re < 4,000$) using DPIV. In *Proceeding of FEDSM'98: 1998 ASME Fluids Division Summer Meeting*, Washington, DC, 1998.

C.H.K. Williamson. Vortex dynamics in the cylinder wake. *Ann. Rev. Fluid Mech.*, **28**:477–539, 1996.